Chapter 1

Nulling Interferometry

E. Serabyn

Jet Propulsion Laboratory, California Institute of Technology,
Pasadena, CA, 91109, USA
gene.serabyn@jpl.nasa.gov

Nulling interferometry uses destructive interference to suppress starlight in order to enhance the contrast of faint emission sources near the target star. Nulling can probe closer to stars than coronagraphy can, thus enabling unique observations of exozodiacal dust and faint companions inside the coronagraphic regime. Nulling has undergone numerous advances recently, both in optical implementation schemes, and in data analysis and calibration approaches, and this chapter provides an overview of the theory, techniques and requirements unique to nulling interferometry. It concludes with a mention of future possibilities.

1. Nulling Interferometry vs. Standard Astronomical Interferometry

The goal of nulling interferometry[1] (or, more simply, "nulling") is to suppress starlight by destructively interfering the light collected by separate telescope apertures or sub-apertures. In general, nulling can differ from standard long-baseline optical/infrared interferometry in several regards, including the beam combination approaches, the fringe measurement, tracking and stabilization methods, and the data processing and calibration techniques. The most basic difference arises from the fact that in normal astronomical interferometry, the determination of the fringe parameters (visibility and phase) is paramount, while the null fringe is typically used primarily to suppress starlight, so as to enhance the observability of much fainter off-axis emission. However, once the star is nulled, interferometry may or may not be used to determine the off-axis source parameters.

For the rejection of starlight to be deep and stable, an achromatic "null fringe" must be kept fixed on the center of the star, which rules out the scanning of the fringe pattern. This means that rather than measuring the fringe visibility, V, *i.e.*,

$$V = \frac{I_{max} - I_{min}}{I_{max} + I_{min}}, \quad (1)$$

where I_{max} and I_{min} are the fringe maximum and minimum, respectively, nullers usually measure a different but related fringe quantity, the null depth, N, given by[2]

$$N = \frac{I_{min}}{I_{max}} . \quad (2)$$

The two are related via

$$V = \frac{1-N}{1+N}, \quad or\ conversely, \quad N = \frac{1-V}{1+V} . \quad (3)$$

The advantage of N is that it directly measures the small quantity desired, *i.e.*, the residual light leakage, whereas visibilities close to unity become difficult to distinguish from unity. In the small null depth limit, we have

$$V \approx 1 - 2N, \quad or\ conversely,\ N \approx \frac{1-V}{2} . \quad (4)$$

As any light leakage will degrade the depth of the fringe minimum, the measured null depth will be astrophysically meaningful only if instrumental leakage terms are minimized and/or removed by calibration.

Finally, we note that, as the nulling of astrophysical sources requires the cancellation of the incident fields to be relatively stable, nulling tends to be easier at longer wavelengths. Indeed, the first nulling observations were carried out in the microwave regime,[3] with the first such observations being of the Sun, as was the case with coronagraphic observations. The nulling of other stars was first proposed for mid-infrared wavelengths,[1] because exoplanets and exozodiacal light are both expected to be bright in the thermal infrared. A number of ground-based nullers aimed at the detection of thermal dust emission at mid-infrared wavelengths have now been deployed,[4-7] and it has also proven possible to extend nulling observations to the near-infrared,[8-10] by taking advantage of extreme adaptive optics systems for wavefront stabilization, and of the very much lower thermal background emission at those wavelengths.

2. Two-Beam Nulling

The simplest case is two-beam nulling. To enable a fringe minimum that is both deep and broadband, the two incoming beams must be combined so as to simultaneously cancel the fields at all wavelengths in the observing passband, and

in both polarization states. For a high degree of cancellation after propagation down the respective optical beam trains, the fields at the beam combiner must be extremely well matched, implying both a high degree of symmetry (for matching, *e.g.*, amplitudes and polarization states) and stability (to keep the relative phase between the beams fixed).

Regardless of the specific beam-combination technique used (see next section), a two-beam nuller combines a pair of beams in anti-phase, yielding linear on-sky fringes that are spaced in angle, as usual, by λ/b, where λ is the observation wavelength and b is the baseline length between the apertures, but with a central achromatic destructive fringe centered on the star (Fig. 1). The on-sky fringe transmission at any wavelength is then

$$t(\theta_\perp) = \frac{1}{2}\left(1 - cos\left(\frac{2\pi b\theta_\perp}{\lambda}\right)\right) = sin^2\left(\frac{\pi b\theta_\perp}{\lambda}\right), \quad (5)$$

where $\theta_\perp$ is the angle on the sky from the central null fringe in the direction perpendicular to the fringes. At large angles, the response is usually reduced (as illustrated in Fig. 1) because of coherence or transmission losses arising from a number of factors such as passband averaging,[11] focal-plane beam combination,[9,10] and/or spatial filtering.[12,13]

With a nulling baseline that can be rotated around the line of sight, the response to a point source located at a radial angular offset from the central star of θ_p and an azimuth angle of α_p is then

$$t(\theta_\mathrm{p}, \alpha) = sin^2\left(\frac{\pi b\theta_\mathrm{p}\, cos\,(\alpha_\mathrm{p} - \alpha)}{\lambda}\right), \quad (6a)$$

where α is azimuth angle of the baseline. Point source response curves for a full 180° of baseline rotation for sources at angular radii of 0.25, 0.5, 0.75 and 1.0 times the fringe spacing are shown in Fig. 1, where it can be seen that point sources at larger radial offsets cause responses containing higher harmonics of the rotation frequency, because more fringes are crossed during the rotation. Frequency and phase analysis of the signal resulting from baseline rotation can thus be used to determine source locations.[14,15,16] However, at small radial offsets, Eq. 6a reduces to

$$t(\theta_\mathrm{p}, \alpha) = \left(\frac{\pi b\theta_\mathrm{p}\, cos\,(\alpha_\mathrm{p} - \alpha)}{\lambda}\right)^2 = \frac{1}{2}\left(\frac{\pi b\theta_\mathrm{p}}{\lambda}\right)^2\left(1 + cos\left(2(\alpha_\mathrm{p} - \alpha)\right)\right), \quad (6b)$$

which has only a single frequency component at twice the baseline rotation frequency. Moreover, as the signal due to a point source is proportional to the product of its flux, F_p, with t, the small-angle signal is proportional to $F_\mathrm{p}\theta_\mathrm{p}^2$, implying a degeneracy at small angles between the source flux and angular offset.

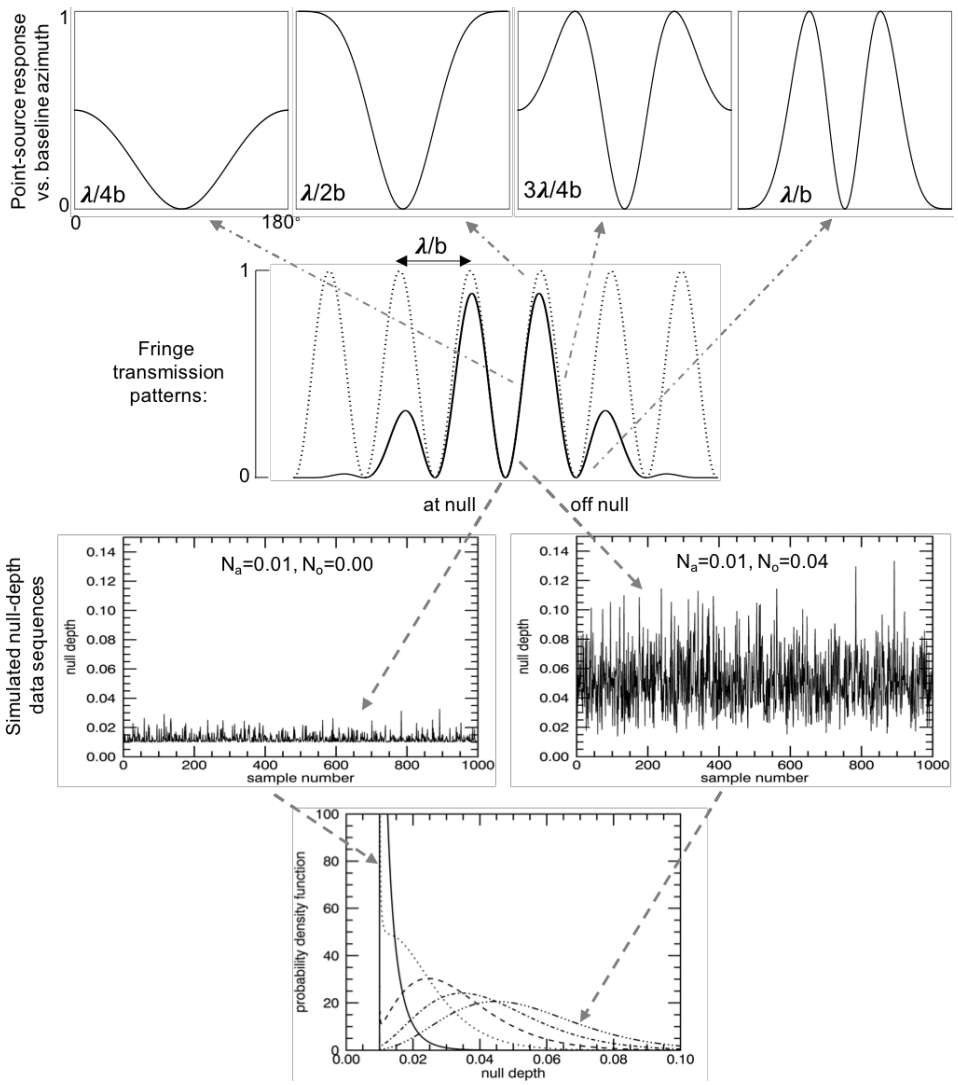

Fig. 1. Second row: A cross-cut through the fringe transmission pattern of a monochromatic single-baseline nuller (dotted line), and a more localized response (solid line) due to, *e.g.*, reduced off-axis coherence or transmission. The null fringe is at the center of the fringe packet. Top row, left to right: Response vs. baseline rotation angle to point sources at radial offsets from the central star of *λ/4b, λ/2b, 3λ/4b* and *λ/b.* (The dash-dotted arrows originate roughly at the largest fringe phases reached during the rotation). Third row: Simulated null-depth data sequences for an astrophysical null depth, N_a, of 0.01, a root-mean-square phase error of 0.1 radians, and mean phases corresponding to null offset leakages of N_o=0.00 (left panel) and 0.04 (right panel). (The two downward-pointing dashed arrows originate roughly at the fringe setpoints.) Bottom: null-depth probability density functions for an astrophysical null of 0.01, a root-mean-square phase error of 0.1 radians, and null offsets (due to phase setpoint errors) of 0.00, 0.01, 0.02, 0.03 and 0.04. The first and last of these curves correspond to the two simulated data sequences shown directly above, as indicated by the dashed arrows.

The response to extended sources is given by the convolution of the "nulled brightness distribution"[13] (*i.e.,* the product of the source brightness distribution with the fringe transmission pattern) with the single-aperture point-source response, which reduces to the integral of the product of the nulled brightness distribution with the centered single-aperture response in the case that spatial filtering is applied.[4,5,12,13,17] Relating measured null depths to circumstellar disk parameters then requires modelling both the source structure and its coupling to the nuller's response pattern.[15,18-22]

The simplest case of an extended source is a stellar disk. With a peak transmission of unity in the monochromatic case, the ideal null depth for a point source separated from the star by a small angle is given by Eq. 6b, and integration over a uniform stellar disk of small diameter θ_S yields a stellar null of [23]

$$N_s = \frac{\pi^2}{16}\left(\frac{b\theta_S}{\lambda}\right)^2. \tag{7}$$

Including limb darkening, one gets[10]

$$N_s = \frac{\pi^2}{16}\left(\frac{b\theta_S}{\lambda}\right)^2 \frac{\left(1-\frac{7A}{15}\right)}{\left(1-\frac{A}{3}\right)}, \tag{8}$$

where $A(\lambda)$ is the limb darkening coefficient. In either case, it can be seen that a small stellar leakage requires a central null fringe much broader than the stellar diameter. Moreover, because starlight leakage through the null fringe increases quadratically toward the stellar rim (Eq. 6b), null depth measurements are sensitive to "edge effects", and so are well suited to measurements of stellar diameters and limb darkening, and in principle can enhance limb spectra relative to the overall stellar disk.

As an example, with a baseline of 85 m, the erstwhile Keck Interferometer Nuller[6,12,13] (KIN) had a fringe spacing of 24 mas at λ = 10 μm and a theoretical stellar null depth of $\approx 10^{-3}$ on a 1 mas diameter star (the approximate diameter of a G star at 10 pc). On the other hand, with a baseline 6 times shorter (14.4 m), the Large Binocular Telescope Interferometer[7,17,21] (LBTI) provides a 10 μm fringe spacing of roughly 140 mas and a stellar null depth of $\approx 3 \times 10^{-5}$ on the same type of star.

Applying the same definition of inner working angle (IWA) to a nuller as is applied to coronagraphs (*i.e.*, the point at which $t(\theta)$ = ½) gives

$$IWA = \frac{\lambda}{4b}. \tag{9}$$

Combining Eqs. 7 and 9 then yields

$$\frac{IWA}{\theta_S} = \frac{\pi}{16\sqrt{N_S}}, \quad (10)$$

showing that the *IWA* moves outward with improving stellar rejection. With a single-baseline nuller, there is thus necessarily a tradeoff between the inner working angle and angular resolution on the one hand (both proportional to b^{-1}) and the stellar leakage (proportional to b^2), due to the baseline length.

One advantage of nulling is that with sufficient accuracy it can enable measurements to be carried out with baselines much shorter than the baselines typically employed for long-baseline visibility measurements. The case of stellar diameter measurements provides a case in point. When using nulling to measure a star's diameter, the accuracy of the diameter measurement is given by[16]

$$\delta\theta_S = \frac{8\lambda^2}{\pi^2\theta_S}\frac{\delta N}{b^2}, \quad (11)$$

where δN is the null-depth measurement accuracy. As the accuracy of a given star's diameter measurement is proportional to $\delta N/b^2$, a more accurate diameter measurement can be obtained either by increasing the baseline length, or by improving the null-depth measurement accuracy. In fact, for a given $\delta\theta_S$, we have $b \propto \sqrt{\delta N}$, *i.e.*, the needed baseline length decreases as the square root of the null depth accuracy. This comparison is a bit oversimplified, as it leaves out factors such as the ability to vary baseline lengths, but nevertheless, the estimated baseline reduction can be quite sizable. For example, improving visibility or null depth accuracies from the 10^{-2} level to 10^{-4} implies that baselines can be reduced by roughly an order of magnitude, a factor large enough to take the needed baseline lengths from the separated-aperture regime (*i.e.*, ~ 100 m) to lengths that can fit within the diameters of large existing and planned single-aperture telescopes (~ 5 – 40 m). Indeed, high-accuracy near-infrared nulling between a pair of subapertures within the pupil of Palomar's Hale telescope[10,24] has enabled stellar diameter measurements with a baseline of only 3.4 m, which is shorter than the length of Michelson's original stellar interferometer.[25] With longer nulling baselines across larger telescope pupils, it is even possible to measure nearby main-sequence stellar diameters (*e.g.*, a G2 star at 10 pc would have a diameter-limited null depth of 3 x 10^{-3} at λ = 2 μm on a 28 m baseline).

2.1. *Beam combination*

Considering the completely symmetric case of combining two identical beams with zero optical path difference between them at an ideal 50/50 beamsplitter,

symmetry and energy conservation demand that half the incident light should emerge from each side of the beamsplitter. However, as the reflected and transmitted fields that are superposed at each of the beamsplitter outputs have equal amplitudes (as a result of the assumed 50/50 split ratio), each of the two net output fields can only equal the single-beam input amplitudes, as is required by energy conservation, if there is a $\pi/2$ phase shift between the reflected and transmitted beams. Thus, symmetry and energy conservation together demand[11,26,27] that ideal 50/50 beamsplitters must introduce $\pi/2$ phase shifts between their reflected and transmitted beams. As such, fringe minima occur only at non-zero optical path differences, resulting in minima that are chromatic. Conversion to an achromatic nuller thus requires the addition of an extra $\pi/2$ radian phase shift between the combining beams, since broadband cancellation requires an achromatic phase difference of π radians. The extra $\pi/2$ of phase can be supplied most simply by passage through unbalanced dielectric media[4,5] (*i.e.*, a longitudinal phase shift), or by making use of a second beamsplitter pass.[28] The first of these is the method used by both the BracewelL Infrared Nulling Cryostat[5] (BLINC) and the LBTI.[7] Standard interferometric pupil-plane beam combination at a single beam splitter also typically includes an extra unbalanced reflection in one of the two beam trains to allow both polarization states to be co-phased simultaneously.[27]

On the other hand, it is possible to have complete symmetry between the two beam trains if a relative phase shift of π radians is supplied upstream of either a dual-pass beamsplitter configuration,[28] or a focal-plane combiner[29,30] (next section). Several methods of directly introducing an achromatic π-radian phase shift exist,[27] including, *e.g.*, anti-symmetric periscopes, the Gouy through-focus phase, a half-period lateral grating translation, orthogonally oriented half wave plates, and geometric phase. A succession of polarizers can also be used to rotate polarization states into opposition, but at the cost of lower efficiency.

The beam intensity ratio is also affected by passage through a beamsplitter, as beamsplitter reflection and transmission coefficients are in general not equal. The fully-symmetric nuller employed by the KIN thus produced matched output intensities with a symmetric pair of beamsplitter passes in which both beams see the common product of the amplitude and reflection coefficients.[28] Any of the intrinsic π phase shifters listed above can then be inserted ahead of a fully symmetric beam combiner to turn it into a nuller by providing the phase shift needed to turn the central constructive fringe into a destructive fringe.

However, all phase shifters have limitations - some are limited to providing only a single fixed value of the phase shift, and many provide chromatic phase shifts. Working under a fluctuating atmosphere or behind imperfect optical beam trains, the relative phase between two incoming beams will fluctuate randomly,

and will also very likely have a chromatic character. The former implies that a fixed phase shift will be inadequate. Moreover, beam amplitudes are likely to differ after propagation down a pair of different beam trains. Active control of amplitude and phase (the latter being carried out much more rapidly than the former), as well as dispersion correction must then be applied for deep, broadband nulling. Dielectric plates or wedges with net thicknesses adjustable by means of rotation or translation, respectively, can supply a variable phase shift, and together with an adjustable air path, can provide broadband dispersion correction.[31] Residual dispersion could in principle be addressed by spectrally dispersed nulling – *i.e.*, nulling a number of narrow spectral channels individually, as the residual dispersion in each resolution element will be lower than across the entire band of interest. The phase offsets from null likely to be present in the individual channels can then be dealt with either by an adaptive nuller[32] that disperses the nulled light onto a deformable mirror that corrects each channel's mean phase, or by the "null self-calibration" data analysis technique[24] (Sec. 3.2), which can extract each channel's true astrophysical null even in the presence of phase offsets.

2.2. *Pupil-plane vs. focal-plane beam combination and the role of optical fibers*

The previous section was concerned primarily with classical beam combination involving free-space optics, in which the pupils of the two beams are superposed at a beamsplitter (Michelson interferometry). This approach is also referred to as coaxial beam combination,[29] because the two beam axes coincide after beam combination. When nulling in the Michelson configuration, energy conservation implies that when one of the beamsplitter outputs is nulled, the other is bright. The bulk of the starlight is thus well-separated from the nulled output. On the other hand, two beams can instead be combined in the focal plane (Fizeau combination). This case is also referred to as multi-axial combination,[29] because the beam axes don't coincide. In this case, all of the starlight reaches the focal plane, with the null fringe in the center of the fringe pattern,[30] and there are no separate nulling and constructive outputs. The bulk of the starlight thus remains in close proximity to the dark region.

Single-mode optical fibers can play important roles in both beam combination schemes, in the high Strehl ratio[a] regime. In coaxial combiners, an optical fiber located in a focal plane after beam combination can be used to filter out pupil-plane wavefront irregularities, and thus improve null depths.[33] In particular, the

[a] See Chapter 1 of this Volume.

presence of differing spatial aberrations in the two beams produces differently-aberrated stellar point spread functions, leading to off-axis light leakage in the combined beam. Very close to the star, most important are pointing mismatches and low order wavefront errors. However, the only phase term that can propagate within a single-mode fiber is the piston phase difference between beams; all other pupil phase errors are filtered out. Even tip-tilt-related phase errors don't propagate in the fiber; they are instead converted to amplitude errors by the dependence of fiber coupling on angle of arrival. A single-mode fiber coupled to the core of the point spread function (PSF) can thus improve stellar rejection considerably,[33] but over a field of view restricted to the PSF core. In contrast, without a fiber, the available field of view is larger, but the null depths are likely to be more modest.

In the Fizeau configuration, the fringes across the focal-plane Airy disk imply that fine sampling would be needed to isolate the deepest part of the central null fringe, if no spatial filtering were applied. A single-mode fiber coupled to the focal plane Airy disk can thus play a critical role in the Fizeau case as well. First, a single-mode fiber can itself function as a beam-combiner, as a pair of focused beams can be coupled into the same fiber mode if both arrive within the fiber's acceptance cone.[29,30] Moreover, by including an upstream relative phase shift of π between the beams to be combined, the fiber-combiner becomes a nuller, because the resultant anti-phased pair of stellar electric fields produces an anti-symmetric focal-plane field distribution on the fiber input plane that cannot couple to the single-mode fiber's symmetric propagation mode.[29,30] However, while the on-axis starlight cannot couple to the fiber, off-axis emission arriving with a different phase shift can. Because of its relative simplicity, this type of "fiber nuller" was employed by the Palomar Fiber Nuller (PFN).[9,10,16]

3. Instrumental Limitations

Thus far, only the case of an ideal, error-free, two-beam nuller has been discussed. However, in any real interferometer, a number of different types of imperfection can lead to an increased level of light leakage. Since the electric fields at the outputs of the two beam trains must cancel to high accuracy, *i.e.,* $\bar{E}_1 + \bar{E}_2 e^{i\varphi} \approx 0$, the fields must be matched in amplitude, phase, polarization rotation angle, retardance, and dispersion. For the case of monochromatic, single-polarization light, it can be shown that leakages linear in amplitude and phase errors vanish at null, leaving only smaller quadratic leakage terms.[16] This minimum-noise condition is the reason for operating at null, although it does not apply if thermal background noise dominates. To avoid increased noise from other fringe phases, only intensities from the null phase can then be used. As a result, the null is best

calibrated using individual beam intensities rather than data from other fringe phases.

In the Michelson case, the null depth integrated over the combined beam pupil is given by

$$N = N_2(\vec{b}) + N_S(b) + N_\mathrm{i}\,, \tag{12}$$

where the first term is the desired astrophysical signal due to non-stellar off-axis emission, the second is due to stellar leakage, and the third is due to any and all instrumental leakage terms, given in short by[13]

$$N_\mathrm{i} = \tfrac{1}{4}\sum \varepsilon_\mathrm{j}^2\,, \tag{13}$$

which is one quarter of the sum of the variances due to each of the possible leakage sources. In more detail, in an integration time, t, and in the absence of beam shear, the instrumental null is given by[13,23]

$$N_i = \tfrac{1}{4}\left(\overline{\phi_\mathrm{a}^2} + \overline{\phi_\mathrm{t}^2} + \overline{\phi_\mathrm{d}^2} + \overline{\phi_\mathrm{r}^2} + \overline{\alpha^2} + \overline{\delta^2}\right), \tag{14}$$

where the different terms give, in order, the spatial variance of the wavefront phase difference across the beam apertures, the temporal variance of the average phase difference within an integration time, the spectral variance of the dispersion across the passband, the variance of the retardance between the two polarization states, the variance of the residual polarization rotation angle between the beams, and the variance of the amplitude imbalance. Note that each of these variances is taken over a different variable, and the timescales involved can also be quite different, as some terms are relatively stable, while others can vary rapidly.

3.1. *Phase errors*

Due to fluctuations in any of the quantities contributing to the instrumental null depth (Eq. 14), measured null depths will also fluctuate. And as the dominant error term is often phase fluctuations, accurate astrophysical null depth measurements will require stabilization of the relative phase between beams so as to stay at or near the bottom of the null fringe. However, because all fluctuations from the bottom of the null fringe lead to positive-definite increases in the null depth (Eqs. 12 and 14), any time-average of a single-baseline null-depth measurement sequence will necessarily be biased upward, and thus would provide an inaccurate estimate of the astrophysical null depth, N_a. Indeed, in the simplest case of only phase errors about the fringe minimum, a better estimate for N_a would instead

simply be the minimum null depth present in a sequence, as can be seen in the left-hand simulated null-depth measurement sequence in Fig. 1.

This can be seen in more detail by considering Gaussian phase noise, and neglecting all other error sources. In this case, the measured null, N_{m}, at any time is given by

$$N_{\mathrm{m}} = N_{\mathrm{a}} + N_{\mathrm{i}} = N_{\mathrm{a}} + \left(\frac{\phi}{2}\right)^2, \tag{15}$$

where $N_{\mathrm{i}} = (\phi/2)^2$ is the quadratic instrumental phase-error contribution to the measured null depth. In this case, the mean null depth over a measurement sequence is given by[16]

$$\bar{N}_{\mathrm{m}} = N_{\mathrm{a}} + \bar{N}_{\mathrm{i}} = N_{\mathrm{a}} + \frac{\bar{\phi}^2}{4} + \frac{\sigma_\phi^2}{4}, \tag{16}$$

where $\bar{\phi}$ is the mean phase offset from the perfect null phase of π radians (due to, *e.g.*, an experimental set-point error), and σ_ϕ is the root-mean-square phase fluctuation about the mean phase. As Eq. 16 shows, the average measured two-beam null depth is always larger than the true astrophysical null depth because of two factors: the mean phase offset from null, and the variance of the phase fluctuations.

If the two positive bias terms in Eq. 16 were known or measured, they could be subtracted from the measured mean null depth to retrieve the astrophysical null. However, determining the two bias terms is non-trivial, especially as they are specified in terms of phase, rather than null depth, which depends on the square of the phase. However, after some manipulation[16], the last equation can be recast in terms of the root-mean-square null-depth fluctuation, σ_{N}, as

$$\bar{N}_{\mathrm{m}} = N_{\mathrm{a}} + \frac{\sqrt{\bar{\phi}^4 + 8\sigma_{\mathrm{N}}^2}}{4}, \tag{17}$$

using

$$\sigma_{\mathrm{N}}^2 = \frac{\sigma_\phi^4 + 2\sigma_\phi^2\bar{\phi}^2}{8}. \tag{18}$$

Finally, inverting Eq. 17 gives the astrophysical null depth as

$$N_{\mathrm{a}} = \bar{N}_{\mathrm{m}} - \frac{\sqrt{\bar{\phi}^4 + 8\sigma_{\mathrm{N}}^2}}{4}. \tag{19a}$$

In the absence of a mean phase offset error (*i.e.*, for a perfect phase setpoint at the bottom of the null fringe), Eq. 19a simplifies to

$$N_{\mathrm{a}} = \overline{N}_{\mathrm{m}} - \frac{\sigma_{\mathrm{N}}}{\sqrt{2}}\,. \tag{19b}$$

In this case, both of the quantities on the right-hand side are directly calculable from a given null depth measurement sequence, as a result of which the astrophysical null can be determined directly from the data. On the other hand, in the opposite case of a phase offset but no fluctuations, Eq. 19a simplifies to

$$N_{\mathrm{a}} = \overline{N}_{\mathrm{m}} - \frac{\bar{\phi}^2}{4}. \tag{19c}$$

From Eqs. 19a and 19c, it is clear that solving for the astrophysical null also requires accurate knowledge of the mean phase offset between beams during the measurement sequence. In the ideal case, the mean phase offset could be removed by observing, under identical conditions, a calibrator star with no astrophysical contribution to the null depth. However, in practice the mean phase offset is unlikely to remain unaltered from star to star.

Before discussing how to determine the mean phase offset between the beams, it is important to note that Eq. 19a (and the simpler Eq. 19b) links the astrophysical null depth to the variance of the null-depth fluctuations. In other words, in the absence of perfect stabilization at the bottom of the null fringe, the statistics of the null-depth fluctuations become integral to the determination of the astrophysical null depth. This is because of the underlying nonlinear fringe shape, which makes the character of the null depth fluctuations a function of the mean phase offset between the two beams. This is illustrated by the pair of simulated null-depth data sequences shown in Fig. 1, where one can see that all null-depth fluctuations are necessarily positive when starting from the bottom of the null fringe, while for other mean phase offsets, the null-depth can fluctuate in either direction. Indeed, it is the mean-phase-dependent character of the null-depth fluctuations that allows one to distinguish between a true astrophysical null-leakage signal and the null-depth offset caused by a mean phase error (see Sec. 3.2).

However, what is the expected level of null depth fluctuations? In the case of a phase setpoint exactly at null, converting the variance of the phase fluctuations in Eq. 18 to the variance of the optical path difference, σ_x, gives

$$\sigma_{\mathrm{N}} = \sqrt{2}\left(\frac{\pi\sigma_x}{\lambda}\right)^2. \tag{20}$$

Whether pathlengths between separated apertures are stabilized by a fringe tracker, or pathlengths between subapertures within a common telescope pupil by an adaptive optics system, $\sigma_x \sim 100$ nm can be chosen as representative, for which

$$\sigma_{\mathrm{N}} \sim \frac{0.14}{\lambda_{\mu\mathrm{m}}^2}, \tag{21}$$

where $\lambda_{\mu m}$ is the observing wavelength in microns. From the point of view of phase, long wavelengths are thus clearly easier to null, as typical rms null depths (without further phase-stabilization steps) are predicted to be ~ 0.03 at K band (2.2 μm), and ~ 10^{-3} at N-band (10 μm). Note that the first value is roughly consistent with typical K-band visibilities of a few percent. Even deeper mean instrumental null depths thus require even finer phase control, such as phase-averaging over apertures larger than those of the wavefront sensor, or using shorter-wavelength fringe information to stabilize longer-wavelength fringes.[34,35]

However, the mean null depth and the variance of the null are not the full story, as one could presumably use only the deepest null depths in a sequence to delimit faint underlying astrophysical signals (*i.e.*, "lucky" nulling). One must thus ask how often instrumental nulls of a given depth are expected to occur, and how much deeper than the mean null it is possible to probe effectively. For Gaussian phase fluctuations centered at the optimal null phase, the probability, p, of the null depth being below a given level N_x at any time is given by the error function

$$p(N < N_x) = Erf\left(\frac{\sqrt{2N_x}}{\sigma_\emptyset}\right). \tag{22}$$

For the same 100 nm rms phase error as before, K band nulls of 10^{-1}, 10^{-2}, 10^{-3} and 10^{-4} should thus be seen 97%, 50%, 17%, and 5% of the time, respectively, implying that nulls even two orders of magnitude deeper than the average null are present on the order of 10% of the time. At N band, the situation is again much more favorable, with phase fluctuations alone allowing 10^{-4} and 10^{-5} nulls 26% and 8% of the time, respectively. Inclusion of other error terms, and of thermal infrared background noise will of course further limit performance.

3.2. *The null-depth probability density function*

As null depths significantly deeper than the average null should thus appear regularly, the final step is to examine the expected frequency distribution of a set of null-depth measurements. In the simple case where only phase errors are

present, the probability that a given null depth measurement falls within a small range dN is given by

$$p(N)\mathrm{d}N = \sum p(\varphi)\mathrm{d}\varphi\,, \tag{23}$$

where the summation is over the two phases of opposite sign that yield identical null depths. As this equation translates the phase-fluctuation probability density function into the null-depth probability density function, this process can be inverted: *i.e.*, with a measured null depth distribution, and either an assumed or a measured phase distribution function, the astrophysical null N_a can be extracted by fitting the observed null-depth probability distribution.[24,36,37] This procedure has been referred to as the "null self-calibration" (NSC) technique, because the nulling data stream (together with measurements of the individual beam intensities and the dark level) is itself used to extract the calibrated astrophysical null depth. For a quadratic relationship between phase and null-depth as in Eq. 15, and Gaussian phase fluctuations, Eq. 23 implies a null-depth probability density function of

$$p(N) = \sqrt{\frac{2}{\pi(N-N_\mathrm{a})\sigma_\emptyset{}^2}}\; exp\left(\frac{-2(N+N_\mathrm{o}-N_\mathrm{a})}{\sigma_\emptyset{}^2}\right)\; cosh\left(\frac{4\sqrt{N_\mathrm{o}(N-N_\mathrm{a})}}{\sigma_\emptyset{}^2}\right), \tag{24}$$

where N_o is the null-depth offset corresponding to the mean phase offset error. This one-sided function (Fig. 1) is non-zero only for $N > N_\mathrm{a}$, and initially drops sharply from an infinite asymptote at $N = N_\mathrm{a}$ to higher values of N. This distinctively asymmetric function can be fitted to high accuracy to retrieve N_a as well as the mean null-depth offset N_o, and the phase variance σ_ϕ^2. In the absence of a mean phase offset, Eq. 24 reduces to

$$p(N) = \sqrt{\frac{2}{\pi(N-N_\mathrm{a})\sigma_\emptyset{}^2}}\; exp\left(\frac{-2(N-N_\mathrm{a})}{\sigma_\emptyset{}^2}\right), \tag{25}$$

which, as can be seen in Fig. 1, is a one-sided exponential-like function that approaches infinity at $N = N_\mathrm{a}$.

The opposite case of small null-depth fluctuations, δN, about a much larger null-depth offset, N_o, is revealing. In particular, for $\delta N << N_\mathrm{o}$, one can show that

$$p(\delta N) \approx \frac{1}{\sqrt{2\pi N_\mathrm{o}\sigma_\emptyset{}^2}}\, exp\left(\frac{-(\delta N)^2}{2N_\mathrm{o}\sigma_\emptyset{}^2}\right) exp\left(\frac{(\delta N)^3}{4N_\mathrm{o}^2\sigma_\emptyset{}^2}\right), \tag{26}$$

where $\delta N = N - N_a - N_o$. Moreover, in this limit, Eq. 18 reduces to $\sigma_N^2 = N_o \sigma_\phi^2$, so Eq. 26 becomes

$$p(\delta N) \approx \frac{1}{\sqrt{2\pi\sigma_N{}^2}} exp\left(\frac{-(\delta N)^2}{2\sigma_N{}^2}\right) exp\left(\frac{(\delta N)^3}{4N_o\sigma_N{}^2}\right), \quad (27)$$

which is the product of a standard Gaussian probability distribution (with a center at $N_a + N_o$ and a variance of $\sigma_N{}^2 = N_o \sigma_\phi^2$), with an exponential factor close to unity that introduces skewness: because the exponent in the latter factor changes sign with δN, the resultant probability density function is slightly asymmetric about its center, with positive excursions of a given magnitude being slightly more probable than negative excursions of the same size. This is because the quadratic dependence of null depth on phase near the fringe minimum means that adding a given phase fluctuation to the mean phase offset will alter the null depth by a larger amount than subtracting the same phase fluctuation would. Indeed, the non-linear relationship between the null depth and fringe phase makes it possible to determine all of the necessary parameters – the astrophysical null depth, N_a, the variance of the null depth fluctuations, σ_N^2, and the static null depth offset, N_o, that arises from the mean phase offset – by fitting measured probability density distributions to Eq. 27. This would not be possible without the skewness factor present in Eq. 27, as a symmetric Gaussian function can be completely described by only two parameters – its center and width – and in this case, the center location depends only on the sum $N_a + N_o$. However, the skewness factor in Eq. 27 has no dependence on N_a, and so breaks this degeneracy.

Interestingly, the underlying fringe non-linearity allows the retrieval of the astrophysical null depth even for null-depth measurement sequences that are offset significantly above the actual astrophysical null (*e.g.*, the right-hand simulated data sequence of Fig. 1). In this "off-null" case, the null-depth fluctuations are amplified by the increasing fringe slope off the null (note that the second term in Eq. 18 multiplies the phase fluctuation variance by the square of the fringe slope at the mean phase offset), leading to a broadening of the probability density distribution for larger mean-phase offsets (Fig. 1). Of course, once the mean null-depth offset is determined by a first observation sequence, it can be removed by applying the appropriate phase shift to bring the interferometer to null prior to further observations.

Returning now to the general case of Eq. 24, the shape of the probability density distribution can be much more asymmetric (Fig. 1) than the limiting case of Eq. 27, but the basic conclusions regarding the extraction of parameters still apply. Indeed, the NSC fitting technique is even more robust than suggested by this brief discussion, as use of the full NSC technique[24,37] allows the retrieval of all of the dominant error terms, including, *e.g.*, both amplitude and phase errors. As a result, the NSC algorithm has become the standard data reduction technique for both the PFN and the LBTI nullers.

Finally, note that the NSC procedure for finding the true astrophysical null is akin to the coronagraphic "dark speckle" technique[38] for exoplanet detection, in which speckle fluctuation minima are sought. Indeed, as the flux at any image point is determined by the interferometric combination of the beamlets from each of the AO system's deformable mirror elements, the dark speckle technique is based on multi-beam interferometry rather than two-beam interferometry. The null self-calibration technique and the dark speckle technique can thus be viewed as members of a family of related flux measurement techniques.

4. Multi-baseline Nulling

Of course, a single-baseline nuller has limitations, including a rather slow rise in transmission from the central minimum. Moreover, in the thermal infrared regime, two bright signals need to be removed – the stellar flux and the thermal background (including zodiacal emission in the case of space missions) – but statically nulling a star does not remove the incoherent background. To separate off-axis companions and circumstellar dust emission from the background, some type of signal modulation is required, such as synchronized spatial chopping (as at the LBTI[17,37]), or phase modulation between nullers[39,40] (as the KIN used[12,13]). However, the suppression of starlight requires keeping a given nuller's phase fixed at null, which excludes the use of rapid phase modulation within a single-baseline nuller. These issues can all be addressed with interferometer configurations that make use of a larger number of input beams and baselines. Adding baselines can bring several improvements, including changing the shapes of the central null and the surrounding fringe pattern to provide a more rapid angular transition between the regions of deep starlight suppression and high off-axis transmission, decoupling the nulling parameters from the angular resolution to allow higher resolution observations of the residual light, and enabling rapid phase-modulation capabilities to separate the different signal types.

Because different baseline lengths correspond to different fringe frequencies, the incoming fields from multiple nulling baselines can be combined to generate a fringe pattern that has a broader central null and a more rapid transition to higher off-axis transmission.[14] In particular, higher fringe frequencies can be added with amplitudes that lead to cancellation of the lowest order terms in the expansion of the fringe transmission vs. off-axis angle, yielding higher-order nulls with transmissions at small angles proportional to θ^4 or θ^6 instead of the basic θ^2 null provided by a single baseline nuller.[14,41] More-capable linear nulling arrays based on the use of more than two telescopes are thus possible, but for the space-based case, more telescopes implies additional complexity and a higher cost. Moreover,

higher-order nulling still requires fixed phases between the telescopes involved, thus again excluding phase modulation. Finally, some configurations also assume different field strengths for some of the combining beams, which implies either differently-sized collecting apertures, or a more complex, and potentially also inefficient, beam combiner. On the other hand, circular nulling arrays,[42] which can be implemented with relative phases between telescopes of multiples of $2\pi/n$, where n is the number of collecting telescopes, can make use of equal amplitudes, and can also provide equal pathlengths to a central beam combiner. The simplest of these is the three-element array.[43,44] However, for a given number of telescopes, it has been shown that linear configurations can provide the highest-order nulls.[45] Many of these multi-aperture nulling-interferometer configurations were proposed as configurations for potential space-based nulling missions such as the Darwin interferometer[46] and the Terrestrial Planet Finder Interferometer.[47]

Of course, not all of the baselines need to be involved in nulling the star, and different baselines can in fact play different roles, such as nulling on one set of baselines, and imaging the residual light with another set. In particular, shorter baselines can be used to provide deep stellar nulls, while longer baselines can be used to provide high resolution. Combining long and short baselines in a multi-element nulling array can thus provide both desired attributes, and also a phase-modulation capability, if an adjustable phase shift between different nulling baselines is provided.[39,40,48] In the case of phase modulation between a pair of nulling baselines, the dominant noise terms shift to those due to correlated errors.[12,13,48,49] A dual-nuller approach was used by the four-subaperture KIN[6,12,13], although with the roles of the long and short baselines reversed.

Although higher-order nulling has yet to be implemented on the sky, it should be possible in the near future, as a wide variety of nulling configurations can be implemented in straightforward fashion within the pupil of a large ground-based telescope. Indeed, the upcoming 30m-class telescopes are large enough that multiple subapertures can be laid out within their pupils to create essentially any nulling-array configuration desired.[16] In particular, different subapertures within a given telescope pupil can be arranged to provide different baseline lengths, different baseline orientations, differing field amplitudes from differently-sized subapertures, simulated baseline rotation, and phase-shifting between different baselines. As only one telescope is involved, the complexity then resides entirely in the beam combiner. However, multi-axial Fizeau combiners can simultaneously combine more than two beams,[29] thus potentially keeping beam combiners manageable as well.

5. Future possibilities

To date, nulling interferometers have been implemented using both telescope subapertures and separate telescopes, and at both near-infrared and mid-infrared wavelengths. Based on the experience gained with these systems, it is worth asking what the future may hold for nulling. First, as has already been discussed, nulling behind an extreme adaptive optics system is very advantageous, as the AO system operates as the fringe tracker, considerably simplifying the nuller's optical system. Fizeau combination can also allow a simple fiber-based beam-combiner for multi-aperture systems. However, a further simplification is possible behind large telescopes: rather than building a specialized nulling beam-combiner, one can instead potentially implement a nulling mode within an already existing high-contrast coronagraph. As coronagraphs typically include internal focal and pupil planes where coronagraphic masks are inserted, the coronagraphic masks in these planes could simply be replaced by nulling masks. For example, a pair of dielectric phase plates with a relative π phase shift between them, or a pair of "crossed" half wave plates that rotate electric fields into opposition could be inserted into a pupil plane.[27] On the other hand, a phase grating that combines the +1 and -1 orders from the opposite sides of a telescope aperture could be inserted into a focal plane.[50] In such a scenario, a separate nulling-interferometer optical bench is not required; instead, by inserting appropriate nulling masks into the coronagraphic focal and pupil planes, nulling can become one of a number of observational modes provided by a combined high-contrast coronograph/nuller.

This idea is particularly promising in regards to planned 30m-class telescopes, since it can extend the high contrast observational regime of such large telescopes further inward, to an *IWA* approaching $\lambda/4D$, well inside the typical coronagraphic *IWA* of ~ 1-3 λ/D. Nullers can thus be used to investigate both exoplanets and dust very close to stars, including the nature of the near-infrared interferometric visibility deficit seen around several nearby stars that has been attributed to hot inner dust,[51] and to search for long-term radial velocity trend candidates[52] inside the coronagraphic regime. Moreover, as an *IWA* of ~ $\lambda/4D$ is on the order of a few milli-arcseconds in the near-infrared for 30 - 40 m telescopes, direct observation of hot Jupiters also becomes possible. However, such small *IWA*s on long baselines would imply significant stellar leakage, thus potentially calling for multi-subaperture nulling. As mentioned earlier, multi-subaperture nulling configurations should be straightforward to implement on very large telescopes. Of course, large apertures in a ring-like configuration are a natural match to the large Giant Magellan Telescope subapertures.[53] Longer wavelengths also favor larger subapertures from the viewpoint of signal-to-noise ratio. On the

other hand, filled-aperture telescopes provide more configuration flexibility, even allowing for the use of differently-sized subapertures. By taking advantage of planned instrumentation, such as large telescopes, extreme adaptive optics systems, and high-contrast coronagraphic benches, very cost-effective nulling interferometry on large telescopes may thus soon become feasible.

6. Summary

While nulling interferometry is still a relatively new field, new optical techniques and data-analysis algorithms have enabled optical simplifications, stability relaxation, and substantial improvement in measurement accuracies.[10,12,16,17,22,37] This brief chapter could not address all of the issues related to nulling, and so has focused on the basics as much as possible. Many other topics and references have thus been omitted, such as the potential use of integrated optics,[54] as well as the possibility of combining nulling with closure phase.[55]

Although implementing a nulling interferometer has heretofore tended to be rather involved, integrating nulling optics into existing and/or planned high contrast coronagraphs on large telescopes should allow considerable simplification, potentially converting nulling into an additional coronagraphic observing mode, thereby moving it more into the mainstream. Nullers also have significant observational potential, as a nuller on a 30m-class telescope should be able to make observations not only of hot and/or warm dust very close to nearby stars, but also of close companions, such as massive long-term radial-velocity trend candidates inside the coronagraphic regime, and the innermost known hot Jupiters. Nulling on large telescopes can also provide stellar observations such as main-sequence stellar diameters and limb-enhanced spectroscopy. Thus, while space-based nullers capable of providing mid-infrared exoplanet spectra remain in the future, ground-based nullers continue to progress.

This work was carried out at the Jet Propulsion Laboratory, California Institute of Technology, under contract with NASA. I thank M. Colavita, C. Lindensmith and B. Mennesson for comments and discussions.

References

1. R. N. Bracewell, Detecting nonsolar planets by spinning infrared interferometer, *Nature* **274**, 780-781 (1978).

2. E. Serabyn, J. K. Wallace, H. T. Nguyen, E. G. H. Schmidtlin and G. J. Hardy, Nulling interferometry: Working on the dark fringe, in *Optical and IR interferometry from ground and space*, ASP Conf. Ser. Vol. **194**, 437-442 (1999).
3. H. Nakajima, H. Sekiguchi, M. Sawa, K. Kai, S. Kawashima, T. Kosugi, N. Shibuya, N., Shinohara, and Y. Shiomi, The Radiometer and Polarimeters at 80 35 and 17 GHz for Solar observations at Nobeyama, *Pub. Astron. Soc. Japan* **37**, 163-170 (1985).
4. P. M. Hinz, J. R. P. Angel, W. F. Hoffmann, D. W. McCarthy Jr, P. C. McGuire, M. Cheselka, J. L. Hora and N. J. Woolf, Imaging circumstellar environments with a nulling interferometer, *Nature* **395**, 251-253 (1998).
5. P. Hinz, R. Angel, N. Woolf, B. Hoffmann and D. McCarthy, BLINC: a testbed for nulling interferometry in the thermal infrared, Proc. SPIE vol. **4006**, 349-353 (2000).
6. M. M. Colavita, P. L. Wizinowich, R. L. Akeson, S. Ragland, J. M. Woillez, R. Millan-Gabet, E. Serabyn, M. Abajian et al., The Keck Interferometer, *Pub. Astron. Soc. Pac.* **125**, 1226-1264 (2013).
7. P. M. Hinz, D. Defrere, A. Skemer, V. Bailey, J. Stone E. Spalding, A. Vaz, E. Pinna, A. Puglisi, S. Esposito et al., Overview of LBTI: a multipurpose facility for high spatial resolution observations, Proc. SPIE vol. **9907**, 990704 (2016).
8. P. Baudoz, Y. Rabbia, J. Gay, R. Burg, L. Petro, P. Bely, B. Fleury, P.-Y. Madec and F. Charbonnier, Achromatic interfero coronagraphy II. Effective performance on the sky, *Astron. Astrophys. Supp. Ser.* **145**, 341-350 (2000).
9. S. Martin, E. Serabyn, K. Liewer, F. Loya, B. Mennesson, C. Hanot and D. Mawet, The development and applications of a ground-based fiber nulling coronagraph, Proc. SPIE vol. **7013**, 70131Y (2008).
10. B. Mennesson, C. Hanot, E. Serabyn, K. Liewer, S. R. Martin and M. Mawet, High-contrast stellar observations within the diffraction limit at the Palomar Hale telescope, *Astrophys. J.* **743**, 178 (2011).
11. W. A. Traub, Beam combination and fringe measurement, in *Principles of Long Baseline Stellar Interferometry*, ed. P. R. Lawson, JPL Publ. 00-009, 31-58 (2000).
12. M. M. Colavita, E. Serabyn, R. Millan-Gabet, C. D. Koresko, R. L. Akeson, A. J. Booth, B. P. Mennesson, S. D. Ragland, E. C. Appleby, B. C. Berkey et al., The Keck Interferometer Nuller data reduction and on-sky performance, *Pul. Astron. Soc. Pac.* **121**, 1120-1138 (2009).
13. E. Serabyn, B. Mennesson, M. M. Colavita, C. Koresko, and M. J. Kuchner, The Keck Interferometer Nuller, *Astrophys. J.* **748**, 55 (2012).
14. J. R. P. Angel and N. J. Wolf, An imaging nulling interferometer to study extrasolar planets, *Astrophys. J.* **475**, 373-379 (1997).
15. Kühn, J., Mennesson, B., Liewer, K., Martin, S., Loya, F., Millan-Gabet, R. & Serabyn, E., Exploring intermediate (5-40 AU) scales around AB Aurigae with the Palomar Fiber Nuller, *Astrophys. J.* **800**, 55 (2015).
16. E. Serabyn, B. Mennesson, S. Martin, K. Liewer and J. Kühn, Nulling at short wavelengths: Theoretical performance constraints and application to faint companion detection inside the diffraction limit, in prep. (2019).
17. D. Defrere, P. M. Hinz, B. Mennesson, W. F. Hoffmann, R. Millan-Gabet, A. J. Skemer, V. Bailey, W. C. Danchi, E. C. Downey, O. Durney et al., Nulling data reduction and on-sky performance of the Large Binocular Telescope Interferometer, *Astrophys. J.* **824**, 66 (2016).
18. B. Mennesson, E. Serabyn, C. Hanot, S. R. Martin, K. Liewer & D. Mawet, New Constraints on Companions and Dust within a few AU of Vega, *ApJ*, **736**, 14 (2011).

19. R. Millan-Gabet et al., Exozodiacal Dust Levels for Nearby Main–Sequence Stars: A Survey with the Keck Interferometer Nuller, *Astroph. J.* **734**, 67 (2011).
20. B. Mennesson, R. Millan-Gabet, E. Serabyn, M. M. Colavita, O. Absil, G. Bryden, M. Wyatt, W. Danchi, D. Defrere, O. Dore et al., Constraining the Exozodiacal Luminosity Function of Main-sequence Stars: Complete Results from the Keck Nuller Mid-infrared Surveys, *Astroph. J.* **797**, 119 (2014).
21. D. Defrere, P. M. Hinz, A. J. Skemer, G. M. Kennedy, V. P. Bailey, W. F. Hoffmann, B. Mennesson, R. Millan-Gabet, W. C. Danchi, O. Absil et al., First-light LBT nulling interferometric observations: warm exozodiacal dust resolved within a few AU of η Crv, *Astrophys. J.* **799**, 42 (2015).
22. S. Ertel, D. Defrere, P. Hinz, B. Mennesson, G. M. Kennedy, W. C. Danchi, C. Gelino, J. M. Hill, W. F. Hoffmann, G. Rieke et al., The HOSTS Survey – Exozodiacal Dust Measurements for 30 Stars, *Astron. J.* **155**, 194 (2018).
23. E. Serabyn, Nulling interferometry: symmetry requirements and experimental results, Proc. SPIE vol. **4006**, 328-339 (2000).
24. C. Hanot, B. Mennesson, S. Martin, , K. Liewer, F. Loya, D. Mawet, P. Riaud, O. Absil and E. Serabyn, Improving interferometric null depth measurements using statistical distributions: theory and first results with the Palomar Fiber Nuller, *Astroph. J.* **729**, 110 (2011).
25. A. A. Michelson and F. G. Pease, Measurement of the diameter of α Orionis with the interferometer, *Astrophys. J.* **53**, 249-259 (1921).
26. J. D. Phillips and C. Hickey, Beamsplitters for astronomical optical interferometry, Proc. SPIE vol. **2477**, 132-148 (1995).
27. E. Serabyn, *Nulling Interferometry Progress*, in Proc. SPIE vol. **4838**, 594-608 (2003).
28. E. Serabyn and M. M. Colavita, Fully symmetric nulling beam combiners, *Appl. Opt.* **40**, 1668-167, (2001).
29. O. Wallner, J. M. P. Armengol and A. Karlsson, Multi-axial single-mode beam combiner, Proc. SPIE vol. **5491**, 798-805 (2004).
30. P. Haguenauer and E. Serabyn, Deep nulling of laser light with a single-mode-fiber beam combiner, *Appl. Opt.* **45**, 2749-2754 (2006).
31. C. Koresko, B. Mennesson, E. Serabyn, M. Colavita, R. Akeson and M. Swain, Longitudinal dispersion correction for the Keck Interferometer Nuller, Proc. SPIE vol. **4838**, 625-635 (2003).
32. R. D. Peters, O. P. Lay and M. Jeganathan, Broadband phase and intensity compensation with a deformable mirror for an interferometric nuller, *Appl. Opt.* **47**, 3920-3926 (2008).
33. B. Mennesson, M. Ollivier, and C. Ruilier, Use of single-mode waveguides to correct the optical defects of a nulling interferometer, *J. Opt. Soc. Am. A* **19**, 596-602 (2002).
34. M. M. Colavita, Simultaneous water vapor and dry air path length measurements with the Keck Interferometer Nuller, *Pub. Astron. Soc. Pac.* **122**, 712-721 (2010).
35. D. Defrere, P. Hinz, E. Downey, M. Bohm, W. C. Danchi, O. Durney, S. Ertel, J. M. Hill, W. F. Hoffmann, B. Mennesson et al., Simultaneous water vapor and dry air optical path length measurements and compensation with the Large Binocular Telescope Interferometer, Proc. SPIE vol. **9907**, 99071G (2016).
36. B. Mennesson, N. Scott, T. ten Brummelaar, G. Bryden, N. Turner, O. Absil, R. Milan-Gabet, V. Coude de Foresto, J. C. Augerau, S. Ridgewy, J. Lebreton and L. Marion, Expanding the Chara/fluor Hot Disks Survey, *J. Astron. Instr.* **2**, 1340010 (2013).

37. B. Mennesson, D. Defrere, M. Nowak, P. Hinz, R. Milan-Gabet, O. Absil, V. Bailey, G. Bryden, W. Danchi, G. M. Kennedy et al., Making high-accuracy null depth measurements for the LBTI exozodi survey, in Proc. SPIE vol. **9907**, 99070X (2016).
38. A. Labeyrie, Images of exo-planets obtainable from dark speckles in adaptive telescopes, *Astron. and Astrophys*. **298**, 544-548 (1995).
39. O. Absil, A. Karlsson and L. Kaltenegger, Inherent modulation: a fast chopping method for nulling interferometry, Proc. SPIE vol. **4852**, 431-442 (2003).
40. B. Mennesson, A. Leger and M. Ollivier, Direct detection and characterization of extrasolar planets: The Mariotti space interferometer, *Icarus* **178**, 570-588 (2005).
41. Velusamy, T., Beichman, C.A. and Shao, M., A Dual 3-Element Nulling Interferometer for TPF, in *Optical and IR Interferometry from Ground and space*, ASP Conf. Ser. Vol **194**, 430-436 (1999).
42. B. Mennesson and J. M. Mariotti, Array configurations for a space infrared nulling interferometer dedicated to the search for Earthlike extrasolar planets, *Icarus* **128**, 202-212 (1997).
43. A. Karlsson, O. Wallner, J. P. Armengol and O. Absil, Three telescope nuller, based on multi beam injection into single mode waveguide, Proc. SPIE vol. **5491**, 831-841 (2004).
44. G. Serabyn, Nulling interferometry with three telescopes: triple beam-combiners, virtual telescope arrays, and phased arrays, Proc. SPIE vol. **5491**, 1639-1648 (2004).
45. O. Guyon, B. Mennesson, E. Serabyn and S. Martin, Optimal beam combiner design for nulling interferometers, *Pub. Astron. Soc. Pac.* **125**, 951-965 (2013).
46. A. Léger, J. M. Mariotti, B. Mennesson, M. Ollivier, J. L. Puget, D. Rouan, and J. Schneider, The DARWIN project, *Astroph. and Sp. Sci.* **241**, 135-146 (1996).
47. C. A. Beichman, N. J. Woolf and C. Lindensmith, The Terrestrial Planet Finder (TPF): A NASA Origins program to search for habitable planets, JPL publ. **99-3** (1999).
48. O. P. Lay and S. Dubovitsky, Nulling interferometers: the importance of systematic errors and the X-array configuration, Proc. SPIE vol. **5491**, 874-885 (2004).
49. O. P. Lay, Systematic errors in nulling interferometers, *Appl. Opt.* **43**, 6100-6123 (2004).
50. S. Martin, G. Serabyn, K. Liewer and B. Mennesson, Achromatic broadband nulling using a phase grating, *Optica* **4**, 110-113 (2017).
51. O. Absil, D. Defrere, V. Coude du Foresto, E. Di Falco, A. Merand, J.-C. Augereau, S. Ertel, C. Hanot, P. Kervella, B. Mollier et al., A near-infrared interferometric survey of debris-disc stars. III. First statistics based on 42 stars observed with CHARA/FLUOR, *Astron. and Astrophys.* **555**, A104 (2013).
52. J. R. Crepp, J. A. Johnson, A. W. Howard, G. W. Marcy, D. A. Fischer, L. A. Hillenbrand, S. M. Yantek, C. R. Delaney, J. T. Wright, H. T. Isaacson and B. T. Montet, The TRENDS high-contrast imaging survey. I. Three benchmark M dwarfs orbiting solar-type stars *Astroph. J.* **761**, 39 (2012).
53. S. Shectman, GMT overview, Proc. SPIE vol. **7733**, 77331Y (2010).
54. L. Labadie, J.-P. Berger, N. Cvetojevic, R. Haynes, R. Harris, N. Jovanovic, S. Lacour, G. Martin, S. Minardi, G. Perrin, M. Roth, and R. R. Thomson, Astronomical photonics in the context of infrared interferometry and high-resolution spectroscopy, Proc. SPIE vol. **9907**, 990718 (2016).
55. S. Lacour, P. Tuthill, J. D. Monnier, T. Kotani, L. Gauchet and P. Labeye, A new interferometer architecture combining nulling with phase closure measurements, *Mon. Not. Roy. Astron. Soc.* **439**, 4018-4029 (2014).